One-dimensional analytical approach to modelling evaporation and heating of deformed drops

S. Tonini, G.E. Cossali

February 4, 2016

Abstract

A general analytical solution for the steady-state evaporation from deformed liquid drops is proposed. The solution is applicable to classes of drop shapes for which 1-D solution exists. The method is used to find the evaporation rate and local vapour and heat fluxes for general ellipsoidal drops, extending previous available results on spheroids. A direct dependence of the local vapour flux on the surface Gaussian curvature is evidenced. A quantitative evaluation of the effect of drop deformation on the total evaporation rate and the local vapour flux is reported.

1 Nomenclature

Greek symbols

α	species	$-$
β	non-dimensional drop surface	$-$
ϕ, γ, θ	deformation parameters	m
η, ζ	shape parameters	$-$
ρ	*mass* density	kg/m^3
χ	*mass fraction*	$-$
$\varepsilon_y, \varepsilon_z$	aspect ratios	$-$
ξ	ellipsoidal coordinate	m
ψ	heat flux	W/m^2

Roman symbols

A	drop surface area	m^2
a_x, a_y, a_z	ellipsoid half-axes	m
c	specific heat	J/kgK
C_G	Gaussian curvature	$1/m^2$
F, E	incomplete elliptic integrals	$-$
D_v	mass diffusivity	m^2/s
h	scale factors	m
k_{th}	thermal conductivity	W/mK
Le	Lewis number	$-$
m_{ev}	evaporation rate	kg/s
M_0	constant, *equation (13)*	m
n	mass flux	kg/m^2s
n_{ev}^{ad}	non-dimensional mass flux	$-$
n_v	ξ-component of the mass flux	kg/m^2s
Pr	Prandtl number	$-$
R_0	spherical drop radius	m
R_{eq}	equivalent radius	m
Sc	Schmidt number	$-$
T	temperature	K
q	energy flux	W/m^2
$\dot{Q}$	heat rate	W
U	velocity	m/s
u, v	ellipsoidal coordinates	m
x, y, z	Cartesian coordinates	m
Y	non-dimensional evaporation rate	$-$

Subscripts

s	surface	–
∞	infinite	–

Superscripts

g	gas	–
v	vapour	–

2 Introduction

The evaporation process from dispersed drops in gaseous flows is of primary importance in many natural and industrial processes (automotive, aeronautic, fire suppression, painting, medical aerosol, meteorology, etc.) [1], [2]. Although different industrial applications involving drop evaporation are already being developed, still the theoretical knowledge on the mechanisms governing the phase transition and mass/energy transports within the gas phase is not fully understood [3].

Over the decades a wide literature on the modelling of drop evaporation became available, urged by the need to cope with the double aim to relieve on one hand some stringent assumptions imposed by previous models and on the other hand to be CPU efficient, in order to make available accessible predictive tools to investigate the behaviour of complex multi-drop systems [4].

The simplest model for the mass transport from a particle immersed in a gas flow was proposed by Maxwell back in 1877 [5], which suggested that the driving force guiding this mechanism is the difference in vapour concentration between the particle surface and the free stream and the process is exclusively controlled by *species* diffusion mechanism, but in real gas flow a bulk motion of the vapour and gas mixture surrounding the particle (Stefan flow) is present and this convective effect on the phase transition rate must be taken into account to correctly predict the phenomenon [6]. Many other effects on drop evaporation were considered in further studies, for example the heat and mass diffusion in the droplet interior [7], the liquid composition [8], [9], the effect of gas pressure [10], [11], etc.

In case of dispersed drops immersed in convective flow, the extended film model of Abramzon and Sirignano [12], developed more than 20 years ago, remains the most commonly used and, due to its numerical efficiency, it is commonly implemented in CFD codes for multi-drop calculations (particularly for sprays and aerosols).

These CFD numerical models have been further refined over the decades including more complex physical aspects (drop composition, shape, interaction with other drops and/or solid surfaces (see [13], [14] for reference). Due to the complexity of the numerical implementation of these models and the CPU time requested for a single drop test case simulation, they cannot be used for multi-drop system predictions, but only as benchmarking for simpler models to be developed.

Experimental investigation on liquid drops in multi-particle systems has revealed that they are subject to significant shape deformations while interacting with the carrier phase [15], due to the interaction of surface tension and fluid-dynamic stresses on the drop surface [16]. While surface tension force induces a spherical shape, fluid-dynamic forces are the primary sources of drop deformation. This is clearly evident in case of liquid drop with Weber number above 2, typical of spray combustion applications, which are appreciably non-spherical [17]. These observations were confirmed by numerical studies on liquid deformed drops [18], [19].

As shown in [20], the gas flow around the drop causes a peak pressure at the leading edge and a minimum pressure at the equator, that leads to an oblate shape, while the liquid circulation inside the drop induces a deformation towards the prolate shape. When gas phase viscous effects become predominant a deformation towards dimpled shape is also observed.

The effect of drop deformation on phase transition was investigated by [15], [21], [22], evidencing that this is not negligible particularly in case of high Reynolds and Weber numbers, suggesting that it could be taken into account modelling the continuously evolving interface. Previous studies concluded that the evaporation rates are higher for deformed drops [21].

Mashayek [15] suggested a correlation for the rate of evaporation of deformed drops based on the results from numerical simulations, which showed that the mass flux varies along its surface. The author proposed a correlation to express the mass flux as a function of the surface mean curvature.

Recently, a model to calculate the effect of deviation from spherical shape on heat and mass transfer for oblate and prolate drops was developed [22], evidencing a direct dependence of the local vapour flux on the drop surface Gaussian curvature.

Non-spherical shape is an unstable state for a liquid drop and the opposing effects of surface tension and inertia cause periodic or non-periodic variation of the shape, which is referred to as drop oscillation and it is found to

strongly influence heat, momentum and mass transfer between the drop and the surrounding gas [21]. Oscillation can become important in atomisation systems where the liquid is first disintegrated into small ligaments, which then oscillate towards the asymptotic attainment of an equilibrium spherical shape [23].

Starting from the pioneering work of Lamb [24], a considerable amount of work has been done on the dynamics of oscillating drops; *refer to [25], [26], [27], [28], [29], [30], [31], [32], [33] and [34] for reviews on theoretical, numerical and experimental contributions to this field.* Evaporation was found to be strongly influenced by the drop deformation dynamics, whereas no substantial effect of drop dynamics on evaporation was found [35]. The evaporation from free oscillating particles was investigated in [36], showing that the increase in the evaporation rate of an oscillating drop is proportional to the square of the instantaneous surface disturbance amplitude and it is larger for higher oscillation modes, and that the period of oscillation is decreased by evaporation, while the dominant mode of oscillation remains the same as that for a non-evaporating drop.

Recently, the evaporation of spheroidal drops in gaseous atmosphere has been investigated by [37], calculating the exact solution for the instantaneous vapour flux and sensible heat rate under steady-state conditions as function of the increment of surface area respect to iso-volumic spherical drops and capturing the different evaporating mechanisms from oblate and prolate drops.

The aim of the present work, firstly motivated by the necessity to include the above described complex drop evaporation mechanisms in spray numerical simulations through relatively simple sub-models, is to propose a general analytic approach to model the evaporation from deformed droplets. The following sections report a mathematical approach that allows the derivation of analytical expressions for the steady-state evaporation rate and heat rate from a class of drop shapes that allows a mono-dimensional solution of the governing equations. The local vapour flux distribution is obtained for that class of drops and an exact relation with the local Gaussian curvature is found. The solution is then applied to spheroidal and triaxial ellipsoidal drops evaporating in quiescent atmosphere.

3 Modelling the evaporation of deformed droplets

The steady-state evaporation of a liquid drop is usually analysed under some commonly assumed simplifying conditions. Among them, sphericity is one of the most striking, as explained above, and it will be relieved in the present

approach. *Another commonly accepted simplification, which is also assumed in the present work, is to consider constant gas density. This relatively strong assumption, particularly in high temperature gaseous environment, was relieved in [37] and [38] for spherical drops, but that analysis cannot at present be extended to non-spherical drops.*

The species balance equations can be written in general form for a binary (pure liquid) system as [39]:

$$\nabla_j n_j^{(\alpha)} = 0 \tag{1}$$

where the specie mass flux $n_j^{(\alpha)}(\alpha = g, v$ for gas and vapour, respectively) can be written under the form:

$$n_j^{(\alpha)} = \rho U_j \chi^{(\alpha)} - \rho D_v \nabla_j \chi^{(\alpha)} \tag{2}$$

where $\chi^{(\alpha)} = \frac{\rho^{(\alpha)}}{\rho}$ is the mass ratio, D_v the mass diffusivity ($D_v = D_{AB} = D_{BA}$ in binary systems [39]) and U_j is the Stefan flow velocity. *Substituting equations (2) into equations (1) and summing over the index* α, accounting for $\chi^{(v)} + \chi^{(g)} = 1$, yields the usual mass conservation equation:

$$\nabla_j \rho U_j = 0 \tag{3}$$

Assuming still drop surface and neglecting gas diffusion through the liquid drop, the gas flux is nil at drop surface and consequently it must be nil everywhere; then defining $G = \ln\left(\chi^{(g)}\right)$ equation (2) for $\alpha = g$ yields:

$$U_j = D_v \nabla_j G \tag{4}$$

and under the further assumption of constant diffusion coefficients, equation (3) yields the Laplace equation:

$$\nabla^2 G = 0 \tag{5}$$

that in a orthogonal curvilinear coordinate system becomes *(see, for example, [40])*:

$$\sum_j \frac{\partial}{\partial x^j} \frac{g^{1/2}}{h_j^2} \frac{\partial G}{\partial x^j} = 0 \tag{6}$$

where h_j are the scale factors and $g^{1/2} = h_1 h_2 h_3$.

In this work, only the cases where the heat and mass fluxes are orthogonal to the drop surface are studied (1-D problems), then the analysis will be restricted to curvilinear orthogonal coordinate systems (ξ, u, v) where the deformed drop surface is a coordinate surface, defined by the equation $\xi = \xi_0$. Then equation (6) becomes:

$$\frac{\partial}{\partial \xi}\left(\frac{h_u h_v}{h_\xi} \frac{\partial G}{\partial \xi}\right) = 0 \tag{7}$$

where G is only function of ξ.

The boundary conditions imposed here assume uniform vapour partial pressure on the drop surface and at infinity, i.e.:

$$G = G_s = \ln\left(1-\chi_s^{(v)}\right) \text{ on the drop surface} \tag{8}$$

$$G = G_\infty = \ln\left(1-\chi_\infty^{(v)}\right) \text{ at infinity} \tag{9}$$

Integration of equation (7) yields the solution:

$$\frac{\partial G}{\partial \xi} = \frac{h_\xi}{h_u h_v} K(u,v) \tag{10}$$

$$G = K(u,v)\int_{\xi_0}^{\xi} \frac{h_\xi}{h_u h_v} d\xi + G_s \tag{11}$$

where $K(u,v)$ is an arbitrary function of the coordinates (u,v) and (8) was used. Since $\frac{\partial G}{\partial \xi}$ is a function only of ξ, $\frac{h_\xi}{h_u h_v}$ is separable, i.e.:

$$\frac{h_\xi}{h_u h_v} = H(u,v) f(\xi) \tag{12}$$

and substituting into equantion (10) yields:

$$H(u,v) K(u,v) = \frac{1}{f(\xi)}\frac{\partial G}{\partial \xi} = M_0 \tag{13}$$

where M_0 is a constant. The general solution (11) then becomes:

$$G = M_0 \int_{\xi_0}^{\xi} f(\xi)\, d\xi + G_s \tag{14}$$

and the constant M_0 can be found from the B.C. (9):

$$M_0 = \frac{1}{\int_{\xi_0}^{\infty} f(\xi)\, d\xi} \ln\left(\frac{1-\chi_\infty^{(v)}}{1-\chi_s^{(v)}}\right) \tag{15}$$

3.1 Evaporating flux and mass rate

From equations (2) it easily stems that $n_j^{(v)} + n_j^{(g)} = \rho U_j$ and since $n_j^{(g)} = 0$, the ξ-component of the vapour flux is then:

$$n_v = \rho D_v \frac{K(u,v)}{h_u h_v} = \rho D_v \frac{f(\xi)}{h_\xi \int_{\xi_0}^{\infty} f(\xi)\, d\xi} \ln\left(\frac{1-\chi_\infty^{(v)}}{1-\chi_s^{(v)}}\right) \tag{16}$$

where *equations (4), (10), (13) and* (15) have been used.

The evaporation rate is found by integrating the vapour flux over the entire surface:

$$m_{ev} = \int_A n_v dA = 4\pi\rho D_v \; R_{eq} \; \ln\left(\frac{1-\chi_\infty^{(v)}}{1-\chi_s^{(v)}}\right) \tag{17}$$

where $dA = h_u h_v \; du \; dv$ and:

$$R_{eq} = \frac{1}{4\pi}\frac{\int\int \frac{1}{H(u,v)} du dv}{\int_{\xi_0}^{\infty} f(\xi)\, d\xi} \tag{18}$$

is a constant length that only depends on the scale factors (since $H(u,v)$ and $f(\xi)$ only depend on the coordinate system) and on the constant ξ_0 that defines the drop surface.

3.2 The triaxial ellipsoidal drop and a generalisation of previous results

In this section an original application of the above developed theory is reported. Consider a general triaxial ellipsoidal drop, described by the equation: $\frac{x^2}{a_x^2} + \frac{y^2}{a_y^2} + \frac{z^2}{a_z^2} = 1$ where it will always be assumed that $a_x \geq a_y \geq a_z$ (see Figure 1).

It is worth to notice that this case generalises the classical model for a spherical drop ($a_x = a_y = a_z = R_0$), and the available results for spheroidal drops [22], for the prolate ($a_x > a_y = a_z$) and the oblate ($a_x = a_y > a_z$) cases.

The radius R_0 of a spherical drop having the same volume of the ellipsoidal one is given by the relation:

$$R_0^3 = a_x a_y a_z \tag{19}$$

and, defining the two deformation parameters $\varepsilon_y = \frac{a_y}{a_x}$ and $\varepsilon_z = \frac{a_z}{a_x}$ (to notice that $1 \geq \varepsilon_y \geq \varepsilon_z$), the half-axes become:

$$a_x = \frac{R_0}{(\varepsilon_y\varepsilon_z)^{1/3}}; \quad a_y = \varepsilon_y \frac{R_0}{(\varepsilon_y\varepsilon_z)^{1/3}}; \quad a_z = \varepsilon_z \frac{R_0}{(\varepsilon_y\varepsilon_z)^{1/3}} \tag{20}$$

The natural coordinate system to solve the problem is the ellipsoidal coordinate system [40]:

$$\begin{aligned} x^2 &= \frac{\xi^2 u^2 v^2}{\phi^2\gamma^2} \\ y^2 &= \frac{\left(\xi^2-\gamma^2\right)\left(u^2-\gamma^2\right)\left(\gamma^2-v^2\right)}{\theta^2\gamma^2} \\ z^2 &= \frac{\left(\xi^2-\phi^2\right)\left(\phi^2-u^2\right)\left(\phi^2-v^2\right)}{\theta^2\phi^2} \end{aligned} \tag{21}$$

with:

$$0 \leq v^2 \leq \gamma^2 \leq u^2 \leq \phi^2 \leq \xi^2 < +\infty; \quad \theta^2 = \phi^2 - \gamma^2 \tag{22}$$

the parameters θ, ϕ, γ can be related to the ellipsoid axes ($\xi_0^2 = a_x^2, \xi_0^2 - \gamma^2 = a_y^2,\ \xi_0^2 - \phi^2 = a_z^2$) and to the deformation parameters:

$$\gamma^2 = \frac{R_0^2\left(1-\varepsilon_y^2\right)}{\left(\varepsilon_y\varepsilon_z\right)^{2/3}};\ \phi^2 = \frac{R_0^2\left(1-\varepsilon_z^2\right)}{\left(\varepsilon_y\varepsilon_z\right)^{2/3}};\ \theta^2 = \frac{R_0^2\left(\varepsilon_y^2-\varepsilon_z^2\right)}{\left(\varepsilon_y\varepsilon_z\right)^{2/3}} \tag{23}$$

In this coordinate system, $\frac{h_\xi}{h_u h_v}$ is separable [40] and from *equation* (12):

$$f(\xi) = \frac{1}{\sqrt{\left(\xi^2-\phi^2\right)\left(\xi^2-\gamma^2\right)}};\quad H(u,v) = \frac{\sqrt{\left(\phi^2-v^2\right)\left(\gamma^2-v^2\right)\left(\phi^2-u^2\right)\left(u^2-\gamma^2\right)}}{\left(u^2-v^2\right)} \tag{24}$$

From the previous section, the separability of $\frac{h_\xi}{h_u h_v}$ implies the existence of a 1-D solution given by *equation* (14), which in the present case can be written in terms of the incomplete elliptic integral of first kind $F(x,k) = \int_0^x \frac{dt}{\sqrt{(1-k^2t^2)(1-t^2)}}$ (see [41]):

$$G = -\frac{F\left(\frac{\phi}{\xi},k\right) - F\left(\frac{\phi}{\xi_0},k\right)}{F\left(\frac{\phi}{\xi_0},k\right)} \ln\left(\frac{1-\chi_\infty^{(v)}}{1-\chi_s^{(v)}}\right) + G_s \tag{25}$$

The vapour flux can then be evaluated by the general relation (16):

$$n_v = \rho D_v \frac{\phi}{\sqrt{\left(\xi^2-u^2\right)\left(\xi^2-v^2\right)}F\left(\frac{\phi}{\xi_0},k\right)} \ln\left(\frac{1-\chi_\infty^{(v)}}{1-\chi_s^{(v)}}\right) \tag{26}$$

and the evaporation rate is calculated from *equation* (17), where:

$$R_{eq} = \frac{\phi}{F\left(\frac{\phi}{\xi_0},k\right)} = R_0 \frac{\sqrt{\left(1-\varepsilon_z^2\right)}}{\left(\varepsilon_y\varepsilon_z\right)^{1/3} F\left(\sqrt{\left(1-\varepsilon_z^2\right)}, \sqrt{\frac{\left(1-\varepsilon_y^2\right)}{\left(1-\varepsilon_z^2\right)}}\right)} \tag{27}$$

see also the Appendix for the calculation of $\int\int \frac{1}{H(u,v)} dudv$.

As previously mentioned, this result generalises the spherical and spheroidal cases, and Table 1 summarises the available results for the non-dimensional ratio $\frac{R_{eq}}{R_0}$ in terms of the deformation parameters. It is easy to show that the results for spherical and spheroidal drops are limiting case of that for the triaxial ellipsoidal drop.

3.3 Effect of surface curvature on the local vapour flux

In a previous work [22], it was shown that, for spheroidal drops, a general relation exists between the local mass flux and the local Gaussian curvature of the surface. In an orthogonal curvilinear coordinate system, the Gaussian curvature of a surface defined by $\xi = \xi_0$ can generally be calculated as (see [42]):

$$C_G = -\frac{1}{2g^{1/2}}\left[\frac{\partial}{\partial u}\left(\frac{1}{g^{1/2}}\frac{\partial h_v^2}{\partial u}\right) + \frac{\partial}{\partial v}\left(\frac{1}{g^{1/2}}\frac{\partial h_u^2}{\partial u}\right)\right] \tag{28}$$

Table 2 reports the values of C_G for the ellipsoidal drop and the limiting cases.

From equations (16) and (17) the local vapour flux at drop surface ($\xi = \xi_0$) can be written as:

$$n_v = m_{ev} \frac{f(\xi_0)}{h_\xi \int\int \frac{1}{H(u,v)} dudv} \tag{29}$$

For ellipsoidal, spheroidal and spherical drops the integral $\int\int \frac{1}{H(u,v)} dudv$ is always equal to 4π (see Appendix). The scale factor h_ξ, evaluated for $\xi = \xi_0$, the function $f(\xi_0)$ and the non-dimensional heat flux $n_v^{ad} = \frac{4\pi R_0^2 \, f(\xi_0)}{h_\xi \int\int \frac{1}{H(u,v)} dudv}$, written in terms of deformation parameters, are reported in Table 2.

A simple inspection shows that for all the cases the general form of the non-dimensional local vapour flux is:

$$n_v^{ad} = \left(R_0^2 C_G\right)^{1/4} \tag{30}$$

This proportionality between the local vapour flux and the fourth root of the non-dimensional Gaussian curvature $R_0^2 C_G$, already observed in [22] for spheroidal drops, may lead to the conjecture that *equation* (30) could hold for a wider class of drop shapes.

3.4 The thermal problem

The evaluation of the gas temperature distribution and the heat rate exchanged by the deformed drop with its surroundings can be treated in a way similar to that used for the mass transfer problem. The energy equation, neglecting minor terms like dissipation by viscous stress, species excess kinetic energy and work of pressure forces (see [39], p.465 for the complete equation), can be written as:

$$U_j \nabla_j T = \frac{k_{th}}{\rho c} \nabla^2 T \tag{31}$$

Using equations (4) and (10), the integration of equation (31), accounting for equations (12) and (13), yields the 1-D solution:

$$T = e^{\frac{M_0}{Le} \int_{\xi_0}^{\xi} f(\xi) d\xi} B(u,v) + \frac{C(u,v)}{k} \frac{Le}{M_0} \tag{32}$$

where $Le = \frac{Sc}{\mathrm{Pr}} = \frac{k_{th}}{\rho c D_v}$, and $B(u,v)$ and $C(u,v)$ are generic functions of u and v.

Setting the B.C. as :

$$T(\xi_0) = T_s; \quad T(\xi_\infty) = T_\infty \tag{33}$$

yields (using *equation* 15) the solution:

$$T = e^{\frac{M_0}{Le}\int_{\xi_0}^{\xi} f(\xi)d\xi}\frac{(T_s - T_\infty)}{\left(1 - e^{\frac{G_0}{Le}}\right)} + \frac{T_s e^{\frac{G_0}{Le}} - T_\infty}{\left(e^{\frac{G_0}{Le}} - 1\right)} \tag{34}$$

where $G_0 = \ln\left(\frac{1-\chi_\infty^{(v)}}{1-\chi_s^{(v)}}\right)$. The heat flux at drop surface is then:

$$\psi_\xi = -k_{th}\frac{1}{h_\xi}\frac{\partial T}{\partial \xi} = -k_{th}\frac{M_0}{Le}\frac{f(\xi)}{h_\xi}\left(T_s - \frac{T_s e^{\frac{G_0}{Le}} - T_\infty}{\left(e^{\frac{G_0}{Le}} - 1\right)}\right) \tag{35}$$

and the integration over the drop surface yields the heat rate $\dot{Q} = \int_A \psi_\xi dA$; defining the non-dimensional heat rate as $\hat{Q} = \frac{\dot{Q}}{4\pi R_0 k T_\infty}$, the following relation is found:

$$\hat{Q} = \left(\frac{\hat{T}_s - 1}{1 - e^{-Y\frac{R_0}{R_{eq}}}}\right) e^{-Y\frac{R_0}{R_{eq}}} Y \tag{36}$$

where $\hat{T}_s = \frac{T_s}{T_\infty}$ and $Y = \frac{m_{ev}}{4\pi\rho D_v R_0 Le}$. This formula generalises in a remarkably simple way what already found for spherical drops *at* $Re = 0$ (see for example [37]).

4 Results and discussions

The case of a triaxial ellipsoidal drop can be seen as a generalization of the spheroidal (and spherical) drop cases. *Figure 2(a) shows the* $\varepsilon_y - \varepsilon_z$ *plane where, since* $\varepsilon_z \leq \varepsilon_y$*, only the gray region represents possible ellipsoids.*

Introducing the parameters:

$$\eta^2 = \frac{1-\varepsilon_y^2}{1-\varepsilon_z^2}; \quad \zeta = \varepsilon_y\varepsilon_z = \left(\frac{R_0}{a_x}\right)^3 \tag{37}$$

both ranging between 0 and 1, it is possible to classify the various drop shapes *in a simpler way. Figure 2(b) shows the* $\eta - \zeta$ *plane*: i) $\zeta = 1$ corresponds to the spherical drop, *since in this case* $\varepsilon_y = \varepsilon_z = 1$; ii) $\eta = 0$ corresponds to the oblate spheroid, *since* $\varepsilon_y = 1$, and for $\zeta \to 0$ *(i.e.* $\varepsilon_z \to 0$*)* the shape becomes similar to a disk; iii) $\eta = 1$ corresponds to the prolate spheroid, *since* $\varepsilon_y = \varepsilon_z$, and for $\zeta \to 0$ *(i.e.* $\varepsilon_y, \varepsilon_z \to 0$*)* the shape becomes similar to a wire. The limiting cases (disk and wire) may represent the evaporation of a liquid drop exposed to high velocity flow (disk) rather then the evaporation of a liquid ligament (wire).

The evaporation rate is *proportional to* the non-dimensional parameter $\frac{R_{eq}}{R_0}$(see equation 17, where R_0 is the radius of a spherical drop having the same volume) and it can be expressed as a function of η and ζ.

The surface of a general triaxial ellipsoid, having the same volume of a sphere of radius R_0, can be calculated as [41]:

$$S\left(R_0, \varepsilon_y, \varepsilon_z\right) = 2\pi \frac{R_0^2}{\left(\varepsilon_y \varepsilon_z\right)^{2/3}} \left\{ \varepsilon_z^2 + E\left(\varphi, m\right) \varepsilon_y \sqrt{\left(1-\varepsilon_z^2\right)} + F\left(\varphi, m\right) \frac{\varepsilon_y \varepsilon_z^2}{\sqrt{\left(1-\varepsilon_z^2\right)}} \right\} \tag{38}$$

where $E\left(\varphi, k\right)$ is the incomplete elliptical integral of second kind and:

$$\varphi = \arcsin \sqrt{1-\varepsilon_z^2};\ m^2 = \frac{\left(\varepsilon_y^2 - \varepsilon_z^2\right)}{\varepsilon_y^2 \left(1-\varepsilon_z^2\right)} \tag{39}$$

which can be also expressed as a function of ζ and η using equations (37). Figure 3 shows the values of $\frac{R_{eq}}{R_0}$ as a function of the non-dimensional drop surface $\beta = \frac{S}{4\pi R_0^2}$ for different values of the shape parameter η.

The results show that the non-dimensional *parameter* $\frac{R_{eq}}{R_0}$ monotonically increases with the non-dimensional drop surface, β, and with the shape parameter η. Thus, for a non-spherical drop of given volume and surface, the maximum evaporation rate is obtained with the prolate drop ($\eta = 1$), the minimum value with the oblate drop ($\eta = 0$), as reported in [22], whereas intermediate values are found for all the other drop shapes.

The effect of drop shape is shown in Figure 4, which presents the variation of $\frac{R_{eq}}{R_0}$ with the shape parameter η for given values of the non-dimensional drop surface, β. The results show that for drops with shape parameter lower than about 0.8 the evaporation rate is almost *independent of* η (with variations from the corresponding values obtained with the oblate drops lower than 2%) and it only increases with the parameter β. The increase of $\frac{R_{eq}}{R_0}$ with η, for η larger than 0.8, is more evident for drops with higher values of β (i.e. very deformed drops). The maximum difference between the evaporation rates for the prolate drop and the corresponding oblate drops is about 15%, for the range of the parameter β investigated here.

4.1 Local vapour flux

The non-dimensional local vapour flux at drop surface n_v^{ad} is shown in the three graphs of Figure 5, along the $x-y$, $x-z$ and $y-z$ planes, respectively, for different drop shapes having the same volumes; the drawings on top of figure indicate the line along which the local vapour distribution is calculated. The non-dimensional local vapour flux along the three lines for the simplest case of a spherical drop is represented by the solid-thick line $n_v^{ad} = 1$. The figure also reports the local vapour flux for two spheroidal drops corresponding to the oblate drop with $(\varepsilon_y, \varepsilon_z) = (1, 0.25)$ and the prolate drop with $(\varepsilon_y, \varepsilon_z) = (0.5, 0.5)$, plotted with dashed-thick and dot-thick lines, respectively. On the same

figure the non-dimensional local vapour flux for three triaxial ellipsoidal drops is reported. The first one (solid-thin line) corresponds to the case with $(\varepsilon_y, \varepsilon_z) = (0.5, 0.35)$. The dash-thin line describes the local vapour flux for again a triaxial ellipsoidal drop characterised by $(\varepsilon_y, \varepsilon_z) = (0.75, 0.25)$, which shape is closer to the above mentioned oblate case. Finally the dot-thin line describes the local vapour flux for a triaxial ellipsoidal drop with $(\varepsilon_y, \varepsilon_z) = (0.75, 0.5)$, which shape is closer to the above mentioned prolate case.

The graphs show that for the highly deformed triaxial ellipsoidal drop (solid-thin line, $(\varepsilon_y, \varepsilon_z) = (0.5, 0.35)$), the maximum value of the vapour flux corresponds to the point of maximum surface curvature, which is located at $(x, y, z) = (1, 0, 0)$, while the minimum is located at the point of minimum curvature, at $(x, y, z) = (0, 0, 1)$.

Modifying the drop shape (dash-thin line, $(\varepsilon_y, \varepsilon_z) = (0.75, 0.25)$) to get closer to the spheroidal oblate drop, the vapour flux distribution becomes similar to that of the oblate drop (dash-thick line), except on the $x - y$ plane, where the triaxial drop has a non-uniform curvature and consequently the local vapour distribution increases along the x-axis and it reaches its maximum at $(x, y, z) = (1, 0, 0)$.

Modifying the drop shape (dot-thin line, $(\varepsilon_y, \varepsilon_z) = (0.75, 0.5)$) to get closer to the spheroidal prolate drop, the local vapour flux curve moves towards the prolate drop curve (dot-thick line).

Table 3 reports the non-dimensional surface area (β) and the non-dimensional parameter ($\frac{R_{eq}}{R_0}$) for the above selected deformed drops. To notice that the surface areas differ by less than 43% compared to the surface area of the spherical drop having the same volume, whereas the increase of the total non-dimensional evaporation rate due to the drop deviation from the spherical shape is less than 17%. It is important to point out that the maximum local vapour flux is instead almost doubled for deformed drops compared to the spherical case and the maximum local flux for one shape may be up to four times the minimum value.

5 Conclusions

A new analytical model for heat and mass transfer from deformed drops was developed, solving the species and energy conservation equations under steady state conditions.

The total evaporation rate and the local vapour and heat fluxes are predicted for various drop shapes that allow the existence of a 1-D solution. *Explicit equations to predict the vapour mass fraction and temperature distribution*

for the general 1-D problem, the local vapour flux, the heat and evaporation rates are proposed.

The model is applied to spherical, spheroidal and triaxial ellipsoidal drops having the same volume and/or surface area. The results show that the drop deformation enhances both the total and local mass and heat transfer. The evaporation rate from deformed drops having the same volume and surface is maximum for the prolate drop and minimum for the oblate drop, *while intermediate values of evaporation rate are found for the various ellipsoidal drops.*

For this class of drop shapes the local vapour flux is found to be proportional to the fourth root of the surface Gaussian curvature. Large variations of local vapour flux along the drop surface are found in case of highly deformed drops, and they should be taken into account when local heat and mass transfer phenomena occur.

6 Appendix

For the ellipsoidal case, the integral:

$$I = \int\int \frac{1}{H(u,v)} du dv = 8 \int_{\gamma}^{\beta} \int_{0}^{\gamma} \frac{\left(u^2 - v^2\right)}{\sqrt{\left(\beta^2 - u^2\right)\left(u^2 - \gamma^2\right)}\sqrt{\left(\beta^2 - v^2\right)\left(\gamma^2 - v^2\right)}}\, dv\, du \tag{A.1}$$

can be calculated referring to the definition of the complete elliptic integrals of first and second kind [41]:

$$K(k) = \int_0^1 \frac{dt}{\sqrt{1-t^2}\sqrt{1-k^2t^2}} = F(1,k)\,; \quad E(k) = \int_0^1 \frac{\sqrt{1-k^2t^2}}{\sqrt{1-t^2}} dt \tag{A.2}$$

Splitting the integral I as:

$$I = 8\left(I_{v1} I_{u2} - I_{u1} I_{v2}\right) \tag{A.3}$$

and defining $k = \frac{\gamma}{\beta}$ and $k' = \sqrt{1-k^2}$:

$$I_{v1} = \int_0^{\gamma} \frac{dv}{\sqrt{\left(\beta^2 - v^2\right)\left(\gamma^2 - v^2\right)}} = \frac{1}{\beta} K(k) \tag{A.4a}$$

$$I_{u1} = \int_{\gamma}^{\beta} \frac{du}{\sqrt{\left(\beta^2 - u^2\right)\left(u^2 - \gamma^2\right)}} = \frac{1}{\beta} F(1,k') \tag{A.4b}$$

$$I_{v2} = \int_0^{\gamma} \frac{v^2}{\sqrt{\left(\beta^2 - v^2\right)\left(\gamma^2 - v^2\right)}}\, dv = \beta\left[K(k) - E(k)\right] \tag{A.4c}$$

$$I_{u2} = \int_{\gamma}^{\beta} \frac{u^2}{\sqrt{\left(\beta^2 - u^2\right)\left(u^2 - \gamma^2\right)}} du = \beta E(k') \tag{A.4d}$$

Since (see [41], equation 19.7.1):

$$K(k)\,E(k') - K(k')\,K(k) + K(k')\,E(k) = \frac{\pi}{2} \tag{A.5}$$

the integral I is:

$$I = \int \int \frac{1}{H(u,v)} dudv = 4\pi \tag{A.6}$$

References

[1] Popkov, V. A., Dugacheva, G. M., Reshetnyak, V. Y., and Mashnina, N. V., 1995, Purification of praziquantel by the method of directional sublimation, Pharmaceutical Chemistry Journal, 29(6), pp. 420-421.

[2] Zhifu, Z., Guoxiang, W., Bin, C., Liejin, G., and Yueshe, W., 2013, Evaluation of evaporation models for single moving droplet with a high evaporation rate, Powder Technology, 240, pp. 95-102.

[3] C.T. Crowe, M. Sommerfeld, Y. Tsuji, Multiphase flows with droplets and particles, CRC Press, Boca Raton, 1998.

[4] S. Sazhin, Droplets and Sprays, Springer, 2014.

[5] J.C. Maxwell, Diffusion, in: Encyclopaedia Britannica, ninth ed., vol. 7, 1877, p. 214.

[6] N.A. Fuchs, Vaporisation and droplet growth in gaseous media, Pergamon Press, London, 1959.

[7] W.A. Sirignano, Fluid dynamics and transport of droplets and sprays, Cambridge University Press, 1999.

[8] A.Y. Tong, W.A. Sirignano, Multicomponent transient droplet vaporization with internal circulation: integral equation formulation, Numer. Heat Transfer 10 (1986) 253–278.

[9] Y. Zeng, C.F. Lee, Multicomponent-fuel film-vaporization model for multidimensional computations, J. Propulsion and Power 16 (2000) 964-973.

[10] G. Zhu, S.K. Aggarwal, Transient supercritical droplet evaporation with emphasis on the effects of equation of state, Int. J. Heat Mass Transfer 43 (2000) 1157-1171.

[11] S.K. Aggarwal, H.C. Mongia, Multicomponent and high-pressure effects on droplet vaporization, J. Eng. Gas Turbines Power 24 (2002) 248–255.

[12] B. Abramzon, W.A. Sirignano, Droplet vaporization model for spray combustion calculations, Int. J. Heat Mass Transfer 32(9) (1989) 1605-1618.

[13] Nikolopoulos, N., Theodorakakos, A., and Bergeles, G., 2007, A numerical investigation of the evaporation process of a liquid droplet impinging onto a hot substrate, Int. J. Heat Mass Tran., 50(1), pp. 303-319.

[14] Strotos, G., Gavaises, M., Theodorakakos, A., and Bergeles, G., 2008, Numerical investigation on the evaporation of droplets depositing on heated surfaces at low Weber numbers, Int. J. Heat Mass Tran., 51(7), pp. 1516-1529.

[15] F. Mashayek, Dynamics of evaporating drops. Part I: formulation and evaporation model, Int. J. Heat Mass Transfer 44(8) (2001) 1517-1526.

[16] Loth E., Quasi-steady shape and drag of deformable bubbles and drops, International Journal of Multiphase Flow, 2008, 34(6), pp: 523-546.

[17] R.J. Haywood, M. Renksizbulut, G.D. Raithby, Transient deformation and evaporation of droplets at intermediate Reynolds numbers, Int. J. Heat Mass Transfer 37 (9) (1994) 1401–1409.

[18] M. Hase, B. Weigand, Transient heat transfer of deforming droplets at high Reynolds numbers, Int. J. Numerical Methods for Heat & Fluid Flow 14(1) (2004) 85-97.

[19] J. Schlottke, B. Weigand, Direct numerical simulation of evaporating droplets, Journal of Computational Physics 227 (2008) 5215–5237.

[20] Helenbrook B.T., and Edwards C.F., Quasi-steady deformation and drag of uncontaminated liquid drops, International journal of multiphase flow, 2002, 28(10), pp: 1631-1657.

[21] Jeng S.M., and Deng Z., Numerical simulation of deformed droplet dynamics and evaporation, Recent advances in spray combustion: Spray combustion measurements and model simulation, 1996, 2, pp: 305-328.

[22] S. Tonini, G.E. Cossali, An exact solution of the mass transport equations for spheroidal evaporating drops, Int. J. Heat Mass Transfer 60 (2013) 236-240.

[23] M.E. Fraser, W.K. Lu, A.E. Hamielec, R. Murarka, Surface tension measurement on pure liquid iron and nickel by an oscillating drop technique, Metall. Trans. 2 (1971) 817–23.

[24] H. Lamb , Hydrodynamics, 6th ed: Cambridge University Press, 1932.

[25] A. Prosperetti, Free oscillations of drops and bubbles: the initial-value problem, J. Fluid Mech. 100 (1980) 333-347.

[26] J.A. Tsamopoulos, R.A. Brown, Nonlinear oscillations of inviscid drops and bubbles, J. Fluid Mech. 127 (1983) 519-537.

[27] T.S. Lundgren, N.N. Mansour, Oscillations of drops in zero gravity with weak viscous effects, J. Fluid Mech. 194 (1988) 479-510.

[28] T.G. Wang, A.V. Anilkumar, C.P. Lee, Oscillations of liquid drops: results from USML-1 experiments in space, J. Fluid Mech. 308 (1996) 1-14.

[29] F. Mashayek, N. Ashgriz, Nonlinear oscillations of drops with internal circulation, Phys. Fluids 10 (5) (1998) 1071-1082.

[30] E.H. Trinh, D.B. Thiessen, R.G. Holt, Driven and freely decaying nonlinear shape oscillations of drops and bubbles immersed in a liquid: experimental results, J. Fluid Mech. 364 (1998) 253-272.

[31] A. Prosperetti, Linear oscillations of constrained drops, bubbles, and plane liquid surfaces. Phys.Fluids 24 (3) (2012).

[32] G. Brenna, S. Teichtmeister, Linear shape oscillations and polymeric time scales of viscoelastic drops, J. Fluid Mech. 733 (2013) 504-527.

[33] A. Sanyal, S. Basu, R. Kumar, R., Experimental analysis of shape deformation of evaporating droplet using Legendre polynomials, Physics Letters A 378(5) (2014) 539-548.

[34] J. Li, J.Zhang, A theoretical study of the spheroidal droplet evaporation in forced convection, Physics Letters A 378(47) (2014) 3537-3543.

[35] Z.T. Deng, R.J. Litchford, S.M. Jeng, Two-dimensional simulation of droplet evaporation at high pressure, AIAA Paper 29-3122, 1992.

[36] F. Mashayek, Dynamics of evaporating drops. Part II: free oscillations, Int. J. Heat Mass Transfer 44(8) (2001) 1527-1541.

[37] S. Tonini, G.E. Cossali, A novel vaporisation model for a single-component drop in high temperature air streams, Int. J. Therm. Sci. 75 (2014) 194-203.

[38] S. Tonini, G.E. Cossali, An analytical model of liquid drop evaporation in gaseous environment, Int. J. Therm. Sci. 57 (2012) 45-53.

[39] J.C. Slattery, Momentum, Energy and Mass Transfer in Continua, second ed., vol. 482, R. Krieger Publ., New York, 1981.

[40] P. Moon and D.E. Spencer, Field Theory Handbook, Springer-Verlag, Berlin, 2^{nd} Edition, 1988.

[41] F. W. J. Olver, D. W. Lozier, R. F. Boisvert, C. W. Clark, Eds., NIST Handbook of Mathematical Functions, Cambridge University Press, 2010.

[42] J.L. Synge, A. Schild, Tensor calculus, Dover, 1978.

7 List of Tables

shape	$\varepsilon_y = \frac{a_y}{a_x}$	$\varepsilon_z = \frac{a_z}{a_x}$	$\frac{R_{eq}}{R_0}$
sphere	1	1	1
prolate spheroid	$\frac{1}{\varepsilon}$	$\frac{1}{\varepsilon} < 1$	$\frac{\left\|1-\varepsilon^2\right\|^{1/2}}{\varepsilon^{1/3}} \frac{1}{\ln\left(\sqrt{\frac{\varepsilon+1}{\varepsilon-1}}-1\right)-\ln\left(\sqrt{\frac{\varepsilon+1}{\varepsilon-1}}+1\right)}$
oblate spheroid	1	$\varepsilon < 1$	$\frac{\left\|1-\varepsilon^2\right\|^{1/2}}{\varepsilon^{1/3}} \frac{1}{\left\{\pi-2\arctan\left[\sqrt{\frac{1+\varepsilon}{1-\varepsilon}}\right]\right\}}$
triaxial ellipsoid	$\varepsilon_y < 1$	$\varepsilon_z < 1$	$\frac{\sqrt{(1-\varepsilon_z^2)}}{(\varepsilon_y\varepsilon_z)^{1/3} F\left(\sqrt{(1-\varepsilon_z^2)}, \sqrt{\frac{\left(1-\varepsilon_y^2\right)}{\left(1-\varepsilon_z^2\right)}}\right)}$

Table 1. Non-dimensional ratio $\frac{R_{eq}}{R_0}$ for different drop shapes. The parameter ε is equal to the ratio between the spheroid half length along the symmetry axis and the maximum radius.

shape	$f(\xi_0)$	$\frac{1}{h_\xi}$	n_v^{ad}	C_G
sphere	$\frac{1}{R_0^2}$	1	1	$\frac{1}{R_0^2}$
oblate spheroid	$\frac{\varepsilon^{1/3}}{R_0}$	$\frac{\varepsilon^{1/3}}{R_0\lvert1-\varepsilon^2\rvert^{1/2}\sqrt{\left(\frac{1}{1-\varepsilon^2}-\sin^2 u\right)}}$	$\frac{\varepsilon^{2/3}}{\lvert1-\varepsilon^2\rvert^{1/2}\sqrt{\left(\frac{1}{1-\varepsilon^2}-\sin^2 u\right)}}$	$\frac{\varepsilon^{8/3}}{R_0^2\lvert1-\varepsilon^2\rvert^2\left(\frac{1}{1-\varepsilon^2}-\sin^2 u\right)^2}$
prolate spheroid	$\frac{\varepsilon^{1/3}}{R_0}$	$\frac{\varepsilon^{1/3}}{R_0\lvert1-\varepsilon^2\rvert^{1/2}\sqrt{\left(\frac{1}{\varepsilon^2-1}+\sin^2 u\right)}}$	$\frac{\varepsilon^{2/3}}{\lvert1-\varepsilon^2\rvert^{1/2}\sqrt{\left(\frac{1}{\varepsilon^2-1}+\sin^2 u\right)}}$	$\frac{\varepsilon^{8/3}}{R_0^2(\varepsilon^2-1)^2\left[\frac{1}{\varepsilon^2-1}+\sin^2 u\right]^2}$
triaxial ellipsoid	$\frac{1}{R_0^2(\varepsilon_z\varepsilon_y)^{1/3}}$	$\frac{(\varepsilon_z\varepsilon_y)}{\sqrt{\left(1-\left(\frac{u}{\xi_0}\right)^2\right)\left(1-\left(\frac{v}{\xi_0}\right)^2\right)}}$	$\frac{(\varepsilon_z\varepsilon_y)^{2/3}}{\sqrt{\left(1-\left(\frac{u}{\xi_0}\right)^2\right)\left(1-\left(\frac{v}{\xi_0}\right)^2\right)}}$	$\frac{1}{R_0^2}\frac{(\varepsilon_y\varepsilon_z)^{8/3}}{\left(1-\frac{v^2}{\xi_0^2}\right)^2\left(1-\frac{u^2}{\xi_0^2}\right)^2}$

Table 2. Scale factor parameters, non-dimensional local vapour flux and local Gaussian curvature for spherical, spheroidal and triaxial ellipsoidal drops.

Shape	$(\varepsilon_y, \varepsilon_z)$	β	$\frac{R_0}{R_{eq}}$
sphere	$(1, 1)$	1	1
oblate spheroid	$(1, 0.25)$	1.43	1.17
prolate spheroid	$(0.5, 0.5)$	1.08	1.04
triaxial ellipsoid	$(0.5, 0.35)$	1.14	1.08
triaxial ellipsoid	$(0.75, 0.25)$	1.34	1.14
triaxial ellipsoid	$(0.6, 0.5)$	1.06	1.04

Table 3. Aspect ratio, non-dimensional surface (β) and non-dimensional parameter ($\frac{R_0}{R_{eq}}$) for five selected drops of Figure 5.

8 List of Figures

Figure 1. Schematic of triaxial ellipsoidal drop axes.

Figure 2. Schematic representation of ellipsoidal class in terms of aspect ratio parameters*: (a) $\varepsilon_y - \varepsilon_z$ plane, since $\varepsilon_z \leq \varepsilon_y$ only the grey region represents a possible ellipsoid, (b) $\eta - \zeta$ plane.*

Figure 3. Dependence of R_{eq}/R_0 on drop surface area and shape.

Figure 4. Dependence of R_{eq}/R_0 on the shape parameter η for different values of drops surface area.

Figure 5. Local vapour flux along $x-y$, $x-z$ and $y-z$ planes for different drop shapes. The thick lines on the three drawings on top of figure schematically indicate where the local vapour flux is calculated.

Research Highlights

1. A 1-D analytical model for deformed drop evaporation is proposed.
2. The model calculates the evaporation rate for general ellipsoidal drops.
3. The local vapour and heat fluxes are calculated for these classes of drop shapes.
4. A relation of the local vapour flux with the surface Gaussian curvature is found.
5. A comparative analysis is reported for various drop shapes.

One-dimensional analytical approach to modelling evaporation and heating of deformed drops

S. Tonini, G.E. Cossali *

Department of Engineering and Applied Sciences, University of Bergamo, Viale Marconi 5, 24044 Dalmine, Italy

* Corresponding autor.
E-mail address: cossali@unibg.it (G.E. Cossali).

The Authors disclose any actual or potential conflict of interest related to the work presented in the submitted manuscript.

G.E. Cossali
S. Tonini

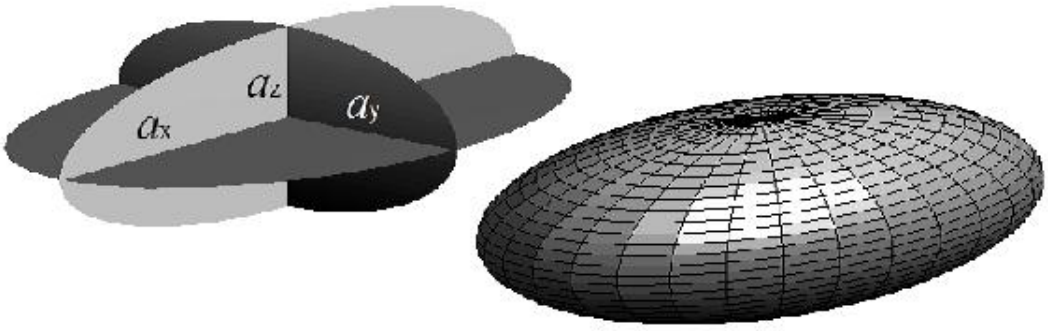
a_z
a_y
a_x

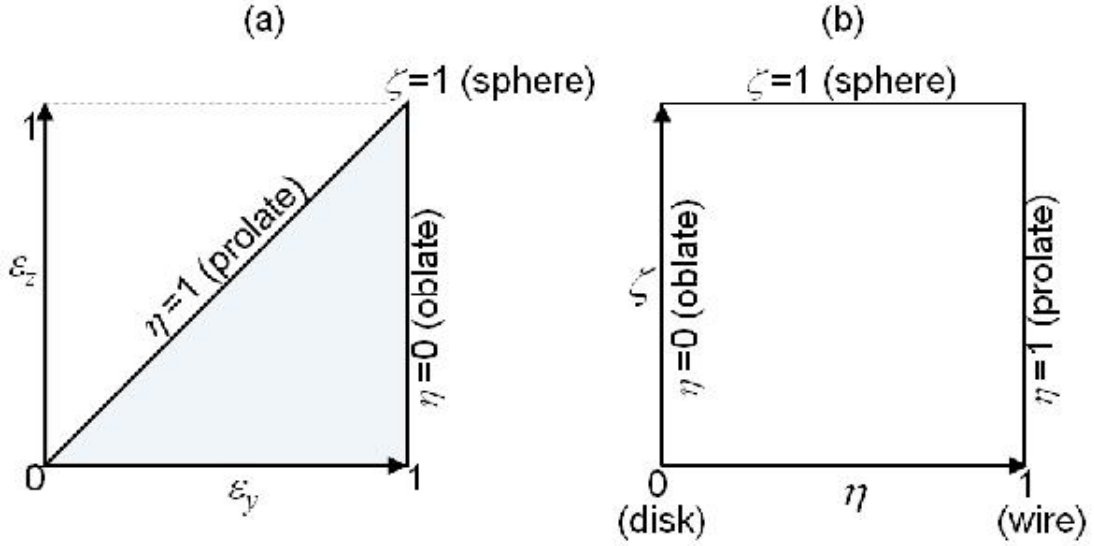
(a)
ζ=1 (sphere)
1
η=1 (prolate)
η=0 (oblate)
0
1
(b)
ζ=1 (sphere)
η=0 (oblate)
η=1 (prolate)
0
(disk)
η
1
(wire)

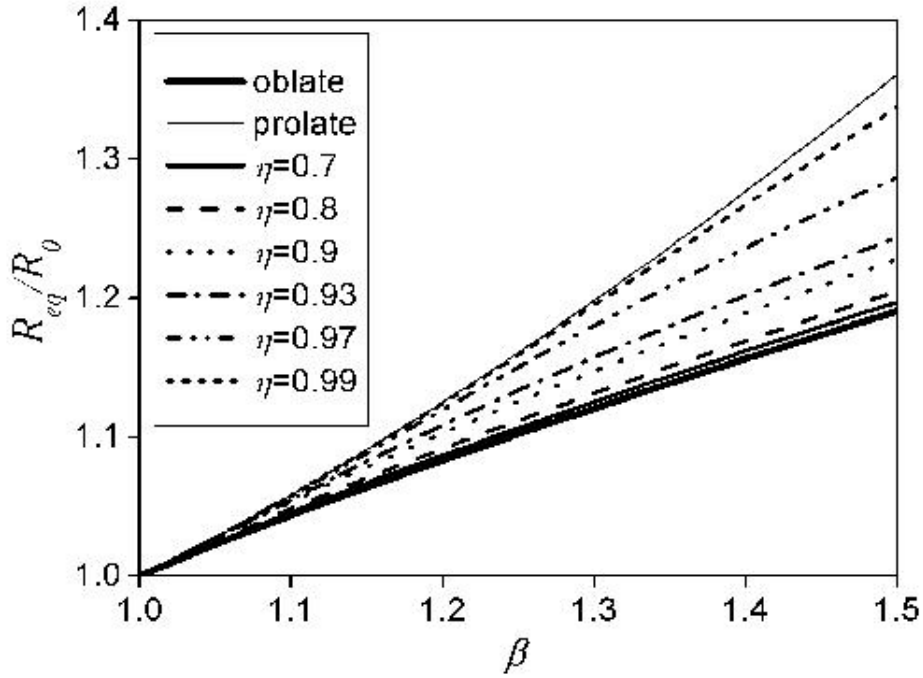
1.4
1.3
1.2
1.1
1.0
1.0
1.1
1.2
1.3
1.4
1.5
R_{eq}/R_0
β
oblate
prolate
η=0.7
η=0.8
η=0.9
η=0.93
η=0.97
η=0.99

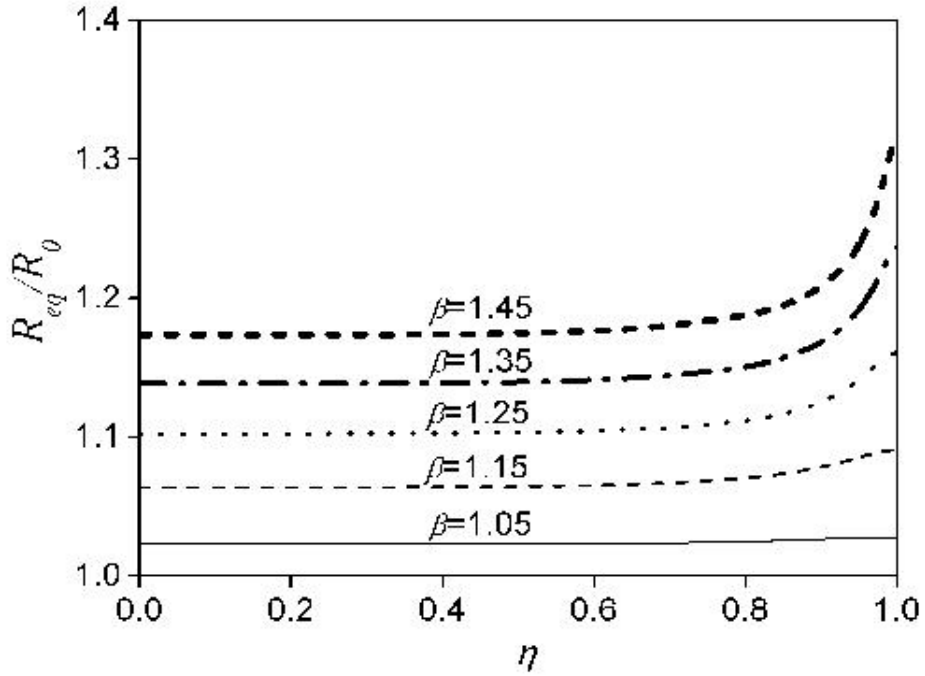
1.4
1.3
1.2
1.1
1.0
R_{eq}/R_0
β=1.45
β=1.35
β=1.25
β=1.15
β=1.05
0.0
0.2
0.4
0.6
0.8
1.0
η

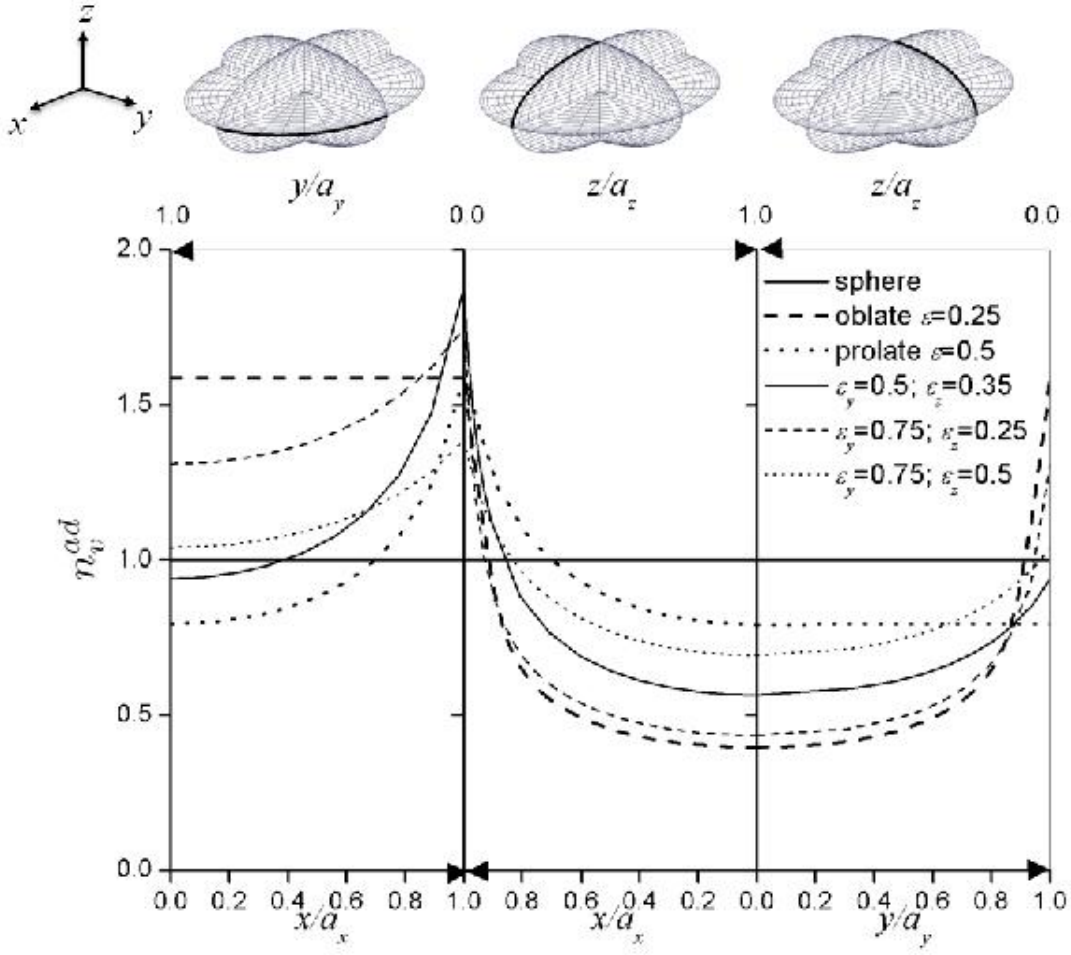
z
x
y
y/a_y
z/a_z
z/a_z
1.0
0.0
1.0
0.0
2.0
1.5
1.0
0.5
0.0
n_v^ad
sphere
oblate ε=0.25
prolate ε=0.5
ε_y=0.5; ε_z=0.35
ε_y=0.75; ε_z=0.25
ε_y=0.75; ε_z=0.5
0.0 0.2 0.4 0.6 0.8 1.0
x/a_x
0.8 0.6 0.4 0.2 0.0
x/a_x
0.2 0.4 0.6 0.8 1.0
y/a_y